Plasmonic Metamaterials Produced by Two-photon-induced Photoreduction Technique

Takuo Tanaka[*1, *2]

[*1] *RIKEN(The Institute of Physical and Chemical Research), Metamaterials Laboratory*
2-1 Hirosawa, Wako, Saitama 351-0198, JAPAN
E-mail: t-tanaka@riken.jp
[*2] *JST PRESTO*

Optical properties of the plasmonic metamaterial that consists of the split ring resonator array are theoretically investigated. Moreover, we propose a micro-fabrication technique that enables us to obtain arbitrary 3D micro/nano metallic structures.

DOI: 10.2961/jlmn.2008.03.0005
Keywords: metamaterials, plasmonics, two-photon-induced reduction, nano-metal

1. Introduction

Plasmonic metamaterial is an artificially designed material whose electromagnetic properties come from its structure. By engineering such materials, we can control their magnetic permeability even in the optical frequency region in which all materials in nature lose magnetic response and their relative permeability is fixed at unity. In this paper, we report on the theoretical investigations of the magnetic response of metamaterials in the visible light region from the viewpoint of the controllability of the permeability. In addition, as a fabrication technique of the plasmoinc metamaterials, we present a two-photon-induced metal-ion reduction technique in a silver-ion aqueous solution, and we demonstrate 3D microstructures with high electrical conductivity, which value is only 3.3 times higher than that of bulk silver.

2. Theory

We have theoretically investigated the magnetic response of plasmonic metamaterials in the optical frequency region [1-3]. Figure 1 shows the split ring-resonator (SRR) model used in our calculations. In Figure 1, r is the radius of the ring, w is the width of the ring, d is the gap distance between two-rings of SRR, J is the induction current, R_s is the surface resistivity, X_s is the internal reactance, a is the unit-cell dimension in the xy plane, and l is the distance between adjacent planes of theSRRs along the z-axis. We derived the effective permeability (μ_{eff}) of the SRRs as

$$\mu_{eff} = \mu_{\mathrm{Re}} + i\mu_{\mathrm{Im}} = 1 - \frac{F\omega^2}{\omega^2 - \frac{1}{CL} + i\frac{Z(\omega)\omega}{L}}, \qquad (1)$$

where C and L are the geometrical capacitance and inductance, and F and $Z(\omega)$ is the filling factor and the ring metal impedance defined by

$$Z(\omega) = \frac{2\pi r}{\omega}\{Rs(\omega) + iXs(\omega)\} \quad \text{and} \quad F = \frac{\pi r^2}{a^2}, \qquad (2)$$

respectively.

By using equation (1) and (2), and taking into account the electro-magnetic properties of the metals (silver, gold, and copper), we calculated the frequency dispersion of μ_{eff} from 100THz to 800THz covering the entire visible light frequency region. As shown in Figure 2(a), at the resonant frequency of the SRR, μ_{eff} changes positively and negatively and it takes max μ_{eff} and min μ_{eff}. In Fig. 2(b), we plotted the calculation results of the change of μ_{eff}, which is defined by the difference between max μ_{eff} and min μ_{eff}, for each metal SRRs array. From these results we have clarified that a three-dimensional array of split-ring-resonators made of silver can give a strong magnetic response in the visible light frequency region. As also shown in Fig. 2(b), silver SRRs exhibit μ_{eff} changes exceeding 2.0 in the entire visible range, which means μ_{eff} can become a negative value, while the responses of gold and copper SRRs do not exceed 2.0 in the visible light region.

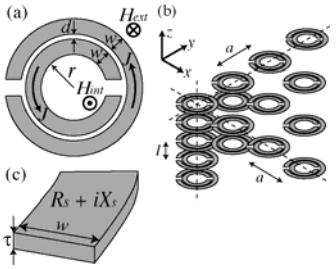

Fig. 1 Figure 1. Calculation Model

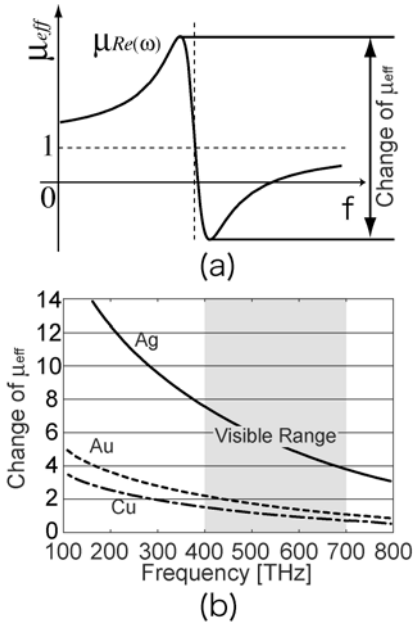

Fig. 2 Frequency dependencies of the change of μ_{eff} of the SRRs.

3. Fabrication technique of plasmonic metamaterials

To create a plasmonic metamaterial structure, the fabrication technique requires the ability to make arbitrary three-dimensional metallic structures. To satisfy this requirement, we have proposed a new fabrication technique that uses two-photon induced reduction of metallic complex ions[4-9].

Figure 3 shows a schematic of this two-photon reduction technique. A mode-locked Ti:Sapphire laser system with a center wavelength of 800 nm, a pulse width of 80 fs, and a repetition frequency of 82 MHz was used as a light source. A drop of metal-ion solution was placed on a cover slip. The laser beam was introduced into an inverted microscope and focused at the interface between the metal-ion solution and the cover slip using an oil-immersion objective lens (60×, NA = 1.42). When the focused laser beam illuminates the metal-ion solution, metal-ions absorb two photons simultaneously and they are reduced to the metals. Owing to the nonlinear properties of two-photon absorption process, only at the laser beam spot this metal reduction process occurs and tiny metal particles are created in the three-dimensional space. The focused laser beam was scanned in two dimensions (x-y scanning) using a pair of galvanometer mirrors, and was also scanned in the longitudinal direction (z-scanning) by translating the objective lens using a computer-controlled motor stage installed in the microscope. Because the laser beam scanning area was limited by the field view of the objective lens, which is up to about 300 μm in diameter, the sample glass substrate was mounted on a computer controlled x-y translation stage in order to extend the fabrication area.

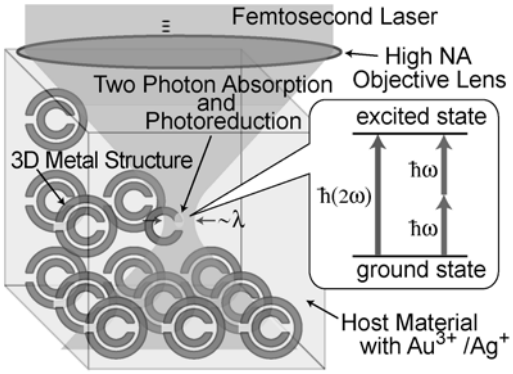

Fig. 3 Schematic of the two-photon reduction technique.

4. Experimental Results

Figure 4 shows two-dimensional metallic structures fabricated on the glass substrates. Fig. 4(a) shows a silver ring structure, and Fig. 4(b) shows a gold ring structure with the same pattern. These photographs were taken using a reflection optical microscope. Fig. 4(c) is a scanning electron micrograph of a magnified portion of the gold ring structure, indicated by the rectangle in Fig. 4(b). The width of the gold line was about 0.7 μm; this value was almost the same as the diameter of the diffraction-limited focused laser beam spot. Note that no metal deposition was observed when mode-locking of the Ti:Sapphire laser was turned off, which substantiates the role of the multiphoton process.

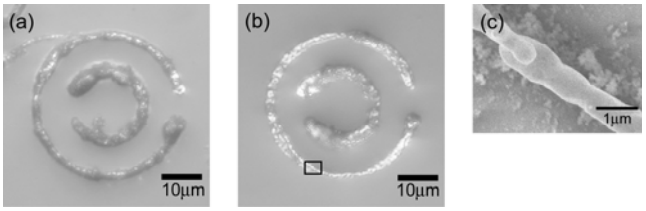

Fig. 4 Double ring structure fabricated on the glass substrate by two-photon-induced metal-ion reduction. (a) Optical microscope image of a silver double ring pattern made by reduction of an $AgNO_3$ aqueous solution. (b) A gold pattern made by reduction of an $HAuCl_4$ solution. (c) Scanning electron micrograph of a part of the gold ring indicated by the rectangle in Fig. (b).

Figure 5 shows the relationship between the size of silver voxels and both the laser power and the exposure time. Figure 5(a) is a scanning electron micrograph of the silver voxels, and Fig. 5(b) shows the dependence of the voxel diameter on the exposure time and laser power. From Fig. 5(b), we found that as the exposure time increases, the diameter of the reduced metal voxel also increases. We also found that there are two trends in the dependences of the voxel diameter on the laser power. If the laser beam power is lower than 6 mW, the increase in diameter is almost linearly proportional to the exposure power for each exposure

time. However, if the exposure power exceeds 6 mW, the degree of increase in diameter declines, and in the 50-ms exposure time case (E), the voxel size is 1.02μm and is almost saturated.

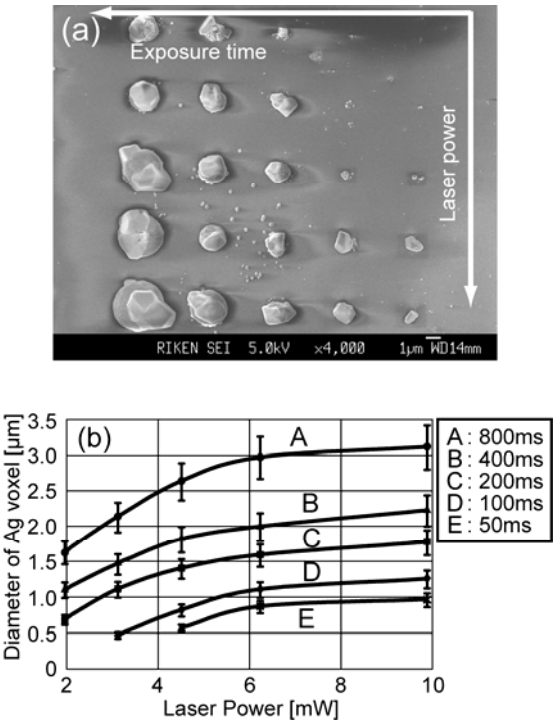

Fig. 5 The relationship between the voxel diameter and both the laser power and the exposure time. (a) Scanning electron micrograph of voxels formed at different laser powers and exposure times. (b) Dependence of voxel diameter on laser power and exposure time.

This is explained as follows. For the metal dots to grow, in addition to the photon energy, a sufficient number of metal ions must exist at the laser beam spot. High-intensity laser irradiation expends the ions quickly and ions are reduced to the metals in the vicinity of laser beam spot, and the resulting lack of metal ions stops further growth of the metal particles. The limited mobility of the ions restricts the supply of ions diffused from the region around the laser spot, thus determining the size of the metal particles. This explanation is supported by the analysis using the diffusion theory and the mobility of Ag-ions in aqueous solution. Figure 6 shows the calculation model, which is in the vicinity of the laser beam spot. According to the Fick's first law [10], the volume of the reduced metal voxel can be expressed as

$$\frac{1}{2} m \frac{4\pi (d/2)^3}{3} = tSD \frac{dc}{dx}, \tag{3}$$

where d is diameter of voxel, m is the density of silver, D is the diffusion coefficient, dc/dx is the gradient of the concentration of ions, t is the exposure time, and S is the surface area of the laser beam spot. To estimate the gradient of the concentration, we assumed that at the center of the laser spot all metal ions were spent out and at the outside of the Airy disk, whose radius is given by

$$r = 0.61 \frac{\lambda}{NA}, \tag{4}$$

no ions were reduced, and then we approximated that the gradient of the concentration was given by C/r, where C is the concentration of silver aqueous solution. Using D = 1.648 x 10^{-9} m^2/s, λ = 800 nm, NA=1.42, t = 50 msec, S = $4\pi r^2$, C = 0.2 mol/l, we finally obtained that the diameter of reduced metal voxel is 1.12 μm [11]. This result has good agreement with the experimental results (1.02 μm).

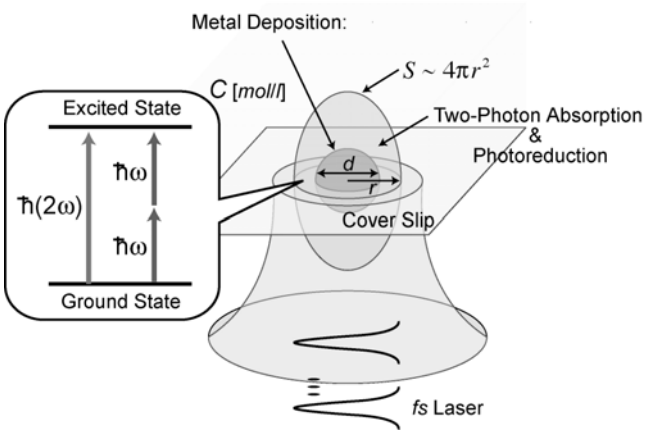

Fig. 6 Calculation model for estimation of the size of two-photon reduced metal voxel.

Figure 7 shows the relationship between laser power and the diameter of the silver wires fabricated on the glass substrate. The scan speed of the laser beam spot was fixed 50 μm/s. As increasing the laser beam power, the line width also increases, and at 7.8mW the degree of increase of the line width changed. This is also explained the same as the size of dots seen in Figure 5. As shown in point (a) in Fig. 7, silver line with 400nm in width was fabricated; this width is smaller than the diameter of the focused laser beam spot.

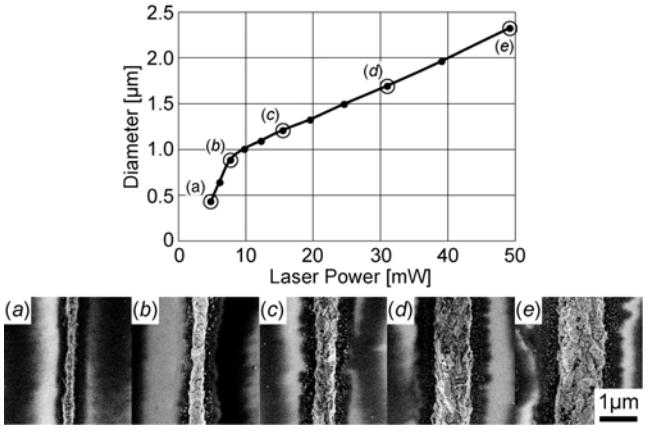

Fig. 7 The relationship between the laser power and the line width of the fabricated silver wiers

To verify the electrical continuity of the metal structure, we measured the resistivity of the fabricated metal wires. Two electrode pads made of silver were fabricated on the glass substrate by electroless plating. A silver wire was then fabricated between these electrodes to connect them. Figure 8(a) is a scanning electron micrograph of the fabricated silver wire and the two electrodes. Figure 8(b) shows a magnified image of the silver wire. As shown in this figure, the fabricated line consisted of silver particles or crystals. The length (l), the width (w), and the height (h) of the wire were estimated from this image. The shape of the cross-section of the line was assumed to be semielliptical, and its area was calculated using w and h, as shown in Fig. 8(c). Figure 8(d) shows the relationship between current and applied voltage for 5 silver wire samples. The gradient of the line corresponds to the resistance. Using measured resistance, length, width, and height for each wire, we have determined that the average of resistivity was 5.30×10^{-8} Ωm. This value is only 3.3 times larger than that of bulk silver (1.62×10^{-8} Ωm), and this indicates the high conductivity of the fabricated silver wires. The discrepancy is due to the roughness and oxidization or sulfurization of the silver wire surface.

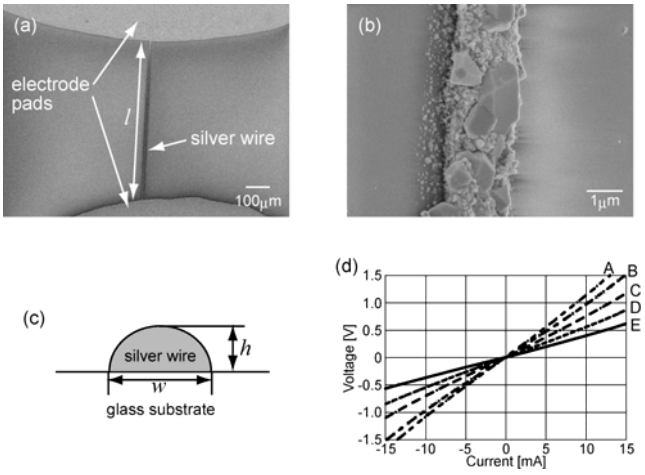

Fig. 8 SEM image of silver wire and electrode pads for measuring the resistivity of the fabricated metal wire (a, b). (c) shows a schematic diagram used to estimate the cross-sectional area of the line. (d) shows the relationship between current and applied voltage. Cross-sectional area and length of sample A, B, C, D, and E were (1.66, 1.57), (1.54, 1.16), (1.49, 1.74), (1.31, 2.63), and (1.75 μm^2, 3.50 mm), respectively.

Figure 9(a) shows silver wires fabricated with a laser power of 4.32 mW and a scan speed of 50 μm/s. Figure 9(b) shows a silver mesh with a total size of 120 μm × 120 μm fabricated with a total exposure time of 12.15 s and a laser power of 13.66 mW.

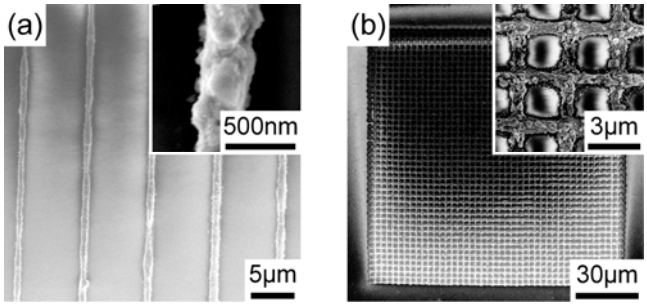

Fig. 9 SEM images of (a) silver wires and (b) silver mesh. The insets show magnified images. The minimum width of the wire with electrical continuity was 400 nm (the inset of Fig. 3(a)). The size of the mesh was 120 μm × 120 μm.

Figure 10 is the scanning electron micrograph of a 3D self-standing silver gate microstructure on a glass substrate. The width, height, and line width of the 3D silver gate are 12, 16, and 2 μm, respectively. The scanning speed of the laser spot during exposure was 24 μm/s. The structure was fabricated as follows. First, two poles were fabricated by scanning the z-stage from the bottom (glass substrate) to the top with a laser power of 18.8 mW. Then, their tops were connected by scanning the laser beam with a laser power of 29.8 mW. The reason for the different laser powers was the different reduction rates of the metal ions at the glass-solution boundary and in the solution, the former being much higher. This mechanism is still not fully understood and needs further investigation.

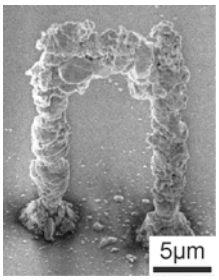

Fig. 10 Scanning electron micrograph of micro-sized 3D silver gate structure standing on a glass substrate without any support. The width, height, and line width were 12, 16, and 2 μm, respectively.

Figure 11 also shows the 3D metal structures fabricated by using silver ion aqueous solution with Coumarin 440. Fig. 11(a) shows a silver tilted rod fabricated with a laser power of 18.85 mW and a total exposure time of 10.24 s. The length of the rod and the angle relative to the substrate were 34.64 μm and 60 degree, respectively. During the fabrication, we could deposit silver three-dimensionally while maintaining a constant angle because of the suppression of the local heating by the dye. We also fabricated a top-heavy silver cup with a laser power of 18.85 mW and a total exposure time of 49.15 s. The height and the top and bottom diameter of the silver cup were 26 μm, 20 μm, and 5 μm, respectively. The strength of the structures produced

was sufficient to fabricate a silver cup that could independently stand on the substrate, as seen in Fig. 11(b).

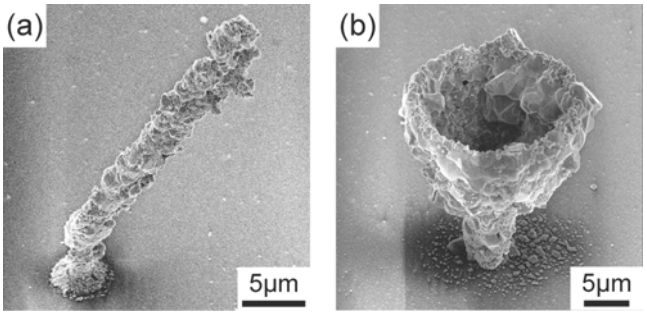

Fig. 11 SEM images of a free-standing (a) silver tilted rod and (b) silver cup on a substrate. The length of the rod and the angle relative to the substrate were 34.64 μm and 60 degree, respectively. The height and the top and bottom diameters of the cup were 26 μm, 20 μm, and 5 μm, respectively.

5. Conclusions

Theoretical investigations on plasmonic metamaterials in the visible light frequency region were reported. This novel material can give us the opportunity to realize unique optical phenomena that never be realized with natural materials. For example, recently we proposed the novel optical components that can realize Brewster condition not only on p-polarized light but also on s-polarized light simultaneously, and this optical component can eliminate the surface reflection completely in spite of the refractive index difference at the interface of the materials [12]. From the technical side, these plasmonic metamaterials should consist of three-dimensional metallic micro/nano structures, but it is difficult to fabricate them by conventional lithography techniques. To solve this problem, we also proposed and developed novel fabrication techniques based on a two-photon reduction process.

References

[1] A. Ishikawa, T. Tanaka, and S. Kawata, Phys. Rev. Lett. **95**, 237401 (2005).
[2] A. Ishikawa, and T. Tanaka, Opt. Commun. **258**, 2, pp. 300-305 (2006).
[3] A. Ishikawa, T. Tanaka, and S. Kawata, J. Opt. Soc. Am. B **24**, 3, pp. 510-515 (2007).
[4] T. Tanaka, A. Ishikawa, and S. Kawata, Appl. Phys. Lett. **88**, 81107 (2006).
[5] A. Ishikawa, T. Tanaka, and S. Kawata, Appl. Phys. Lett. **89**, 113102 (2006).
[6] F. Formanek, N. Takeyasu, T. Tanaka, K. Chiyoda, A. Ishikawa, and S. Kawata, Opt. Express **14**, 2, pp. 800-809 (2006).
[7] F. Formanek, N. Takeyasu, K. Chiyoda, T. Tanaka, A. Ishikawa, and S. Kawata, Appl. Phys. Lett. **88**, 83110 (2006).
[8] J.-F. Xing, X.-Z. Dong, W.-Q. Chen, X.-M. Duan, N. Takeyasu, T. Tanaka, and S. Kawata, Appl. Phys. Lett. **90**, 131106 (2007).
[9] J.-F. Xing, W.-Q. Chen, J. Gu, X.-Z. Dong, N. Takeyasu, T. Tanaka, X.-M. Duan and S. Kawata, J. Mater. Chem., 2007, DOI: 10.1039/b616792f.
[10] J. Crank, The Mathematics of Diffusion 2nd Edi-tion, (Oxford University Press, New York, 1999).
[11] D. R. Lide ed., CRC handbook of chemistry and physics 81st ed. (CRC Press LLC, Boca Raton, 2000).
[12] T. Tanaka, A. Ishikawa, and S. Kawata, Phys. Rev. B **73**, 125423 (2006).

(Received: July 8, 2008, Accepted: October 30, 2008)